

Machine Learning for Automated Quality Assurance in Radiotherapy: A Proof of Principle using EPID Data Description

Issam El Naqa^{1*}, Jim Irrer¹, Tim A Ritter², John DeMarco³, Hania Al-Hallaq⁴, Jeremy Booth⁵, Grace Kim⁶, Ahmad Alkhatib⁷, Richard Popple⁸, Mario Perez⁵, Karl Farrey⁴, and Jean M. Moran¹

¹University of Michigan Department of Radiation Oncology, Ann Arbor, MI 48103, United States of America

²Virginia Commonwealth University Department of Radiation Oncology, Richmond, VA 23298, United States of America

³Department of Radiation Oncology, Cedars-Sinai Medical Center, Los Angeles, California 90048, United States of America

⁴University of Chicago Radiation and Cellular Oncology, Chicago, IL 60637, United States of America

⁵Royal North Shore Hospital, St Leonards, New South Wales 2065, Sydney, Australia

⁶University of California at San Diego, San Diego, CA 92093, United States of America

⁷Karmanos Cancer Institute, McLaren-Flint, Flint, Michigan 48532 United States of America

⁸University of Alabama at Birmingham, Birmingham, AL 35249, United States of America

*Corresponding author: email: ielnaqa@med.umich.edu.

Conflict of interest: Part of this work was supported by Varian Medical Systems (PI: JMM). Otherwise, the authors have no conflicts to disclose with regard to this publication.

This is the author manuscript accepted for publication and has undergone full peer review but has not been through the copyediting, typesetting, pagination and proofreading process, which may lead to differences between this version and the [Version of Record](#). Please cite this article as [doi: 10.1002/MP.13433](https://doi.org/10.1002/MP.13433)

This article is protected by copyright. All rights reserved

Article Type: Research Article

Machine Learning for Automated Quality Assurance in Radiotherapy: A Proof of Principle using EPID Data Description

Issam El Naqa, Jim Irrer, Tim A Ritter, John DeMarco, Hania Al-Hallaq, Jeremy Booth,
Grace Kim, Ahmad Alkhatib, Richard Pople, Mario Perez, Karl Farrey, and Jean M. Moran

Abstract

Purpose: Developing automated methods to identify task-driven quality assurance (QA) procedures is key towards increasing safety, efficacy, and efficiency. We investigate the use of machine learning (ML) methods for possible visualization, automation and targeting of QA, and assess its performance using multi-institutional data.

Methods: To enable automated analysis of QA data given its higher dimensional nature, we used nonlinear kernel mapping with Support Vector Data Description (SVDD) driven approaches. Instead of using labeled data as in typical Support Vector Machine (SVM) applications, which requires exhaustive annotation, we applied a clustering extension of SVDD, which identifies the minimal enclosing hypersphere in the feature space defined by a kernel function separating normal operations from possible failures (i.e., outliers). In our case, QA test data are mapped by a Gaussian kernel to a higher dimensional feature space and then the minimal enclosing sphere was identified. This sphere, when mapped back to the input data space along the principal components, can separate the data into several components, each enclosing a separate cluster of QA points that could be used to evaluate tolerance boundaries and test reliability. We evaluated this approach for gantry sag, radiation field shift, and MLC (multileaf collimator) offset data acquired using electronic portal imaging devices (EPID), as representative examples.

Results: Data from 8 LINACS and 7 institutions (n=119) were collected. A standardized EPID image of a phantom with fiducials provided deviation estimates between the radiation field and phantom center at 4 cardinal gantry angles. Deviation measurements in the horizontal direction (0° , 180°) were used to determine the gantry sag and deviations in the vertical direction (90° , 270°) were used to determine the field shift. These measurements were fed into the SVDD

31 clustering algorithm with varying hypersphere radii (Gaussian widths). For gantry sag analysis,
32 two clusters were identified one of which contained 2.5% of the outliers and also exceeded the
33 1mm tolerance set by TG-142. In the case of field shifts, SVM clustering identified two distinct
34 classes of measurements primarily driven by variations in the second principal component at
35 270°. Results from MLC analysis identified one outlier cluster (0.34%) along Leaf offset
36 Constancy (LoC) axis that coincided with TG-142 limits.

37 **Conclusion:** Machine learning methods based on SVDD clustering are promising for
38 developing automated QA tools and providing insights into their reliability and reproducibility.

39

40 **Keywords:** Machine learning, quality assurance, SVM, Linacs, higher dimension visualization.

41

42

43

44 I. Introduction

45

46 Cancer patients' safety and their treatment outcomes, despite rigorous regulations, may be
47 compromised by rare but deadly errors that can occur during complex treatment planning and
48 delivery of radiotherapy as highlighted by several editorials in national and international media
49 reports in recent years [1]. Traditionally, quality assurance (QA) in radiotherapy follows the
50 guidelines of national and international bodies such as the American Association of Physicists in
51 Medicine (AAPM), American Society for Radiation Oncology (ASTRO), American College of
52 Radiology (ACR), European Society for Radiotherapy and Oncology (ESTRO), and the
53 International Atomic Energy Agency (IAEA). For instance, the AAPM and its widely used task
54 group (TG) report TG-40 [2] has provided a comprehensive QA program for institutional
55 radiation oncology practice. This report accounts for potential risks during the planning and
56 delivery of high energy irradiation, harmonizing the treatment of patients and accommodating
57 new advances in technology. TG-142 updated the requirements for advances in linear accelerator
58 delivery technology[3]. A risk assessment and consensus evaluation of the critical requirements
59 is presented in AAPM Medical Physics Practice Guideline 8a on linear accelerator QA [4].
60 Moreover, QA is a necessary process for credentialing institutions for multi-institutional
61 radiotherapy clinical trials such as the ones carried out by the NRG Oncology consortium and

62 AAPM report TG113 [5-8]. While these QA guidelines have focused on monitoring all
63 functional aspects of radiotherapy equipment, recent efforts have been geared towards
64 identifying failures in workflow and processes. For instance, AAPM TG-100 has taken a risk-
65 based approach using failure mode and effect analysis (FMEA) for designing QA protocols and
66 prioritizing effort [9]. However, whether it is the traditional TG-40/142 or the new TG-100
67 guidelines, both approaches, as useful as they are, remain unfortunately subjective and are
68 opinion-driven rather being data-driven; consequently, physicists are still left without an
69 evidence-based answer to tailor a large number of laborious QA procedures to the associated
70 failure risk. In the era of big data this limitation can be remedied [10,11].

71
72 Radiotherapy provides a fertile environment to harness the power of big data analytics,
73 particularly in areas related to QA and safety [11-13]. Targeting of laborious QA tasks as needed
74 has been recognized as a key component towards safer, more accurate and efficient radiotherapy
75 administration [14]. However, traditional statistical methods cannot handle the challenges posed
76 by radiotherapy big data, particularly the large class imbalance in navigating a great number of
77 variables with a small sample size of relevant clinical data. This is further taken to the extreme in
78 the case of QA, where the event rate is not only small but rare [15], due to improvements in
79 software and hardware functionality and the tremendous efforts performed by the medical
80 physicist. This issue constitutes a serious data analytics challenge.

81
82 Machine learning methods represent the computational vehicle for complex data analytics due to
83 their ability to capture nonlinear and hidden patterns in the data, handle data imbalance, visualize
84 higher dimensional space, and generalize to out-of-sample data [16]. Several studies have
85 utilized different machine learning techniques for QA applications. These applications included
86 automated error checkers of treatment plans using unsupervised learning such as k-means
87 clustering [17] or supervised learning by neural networks [18], Bayesian networks [19], support
88 vector machines (SVM) [20,21], and Poisson regression [22,23]. In addition, ML was applied to
89 linear accelerator (Linac) machine QA such as supervised learning by neural networks of Linac
90 beam symmetry [24] and multi-leaf collimator positional errors by random forest and Cubist
91 methods [25].

92

93 In this work, we recognize that Linac machine QA processes in particular, are typically
94 comprised of laborious tasks that are done based on prescriptive guidelines to monitor machines
95 and equipment performance irrespective of the expected probability of failure risk. Methods
96 based on process control charts have been proposed to assist in longitudinal monitoring of
97 equipment function and separating random from systematic errors by defining action thresholds
98 [14]. However, QA tests consist of multidimensional measures that exhibit complex and
99 potentially nonlinear behavior among them. Thus, we hypothesize that the ability to visualize
100 these tests in a higher dimensional space would allow for better identification of tolerance
101 boundaries and assessment of the ability of these tests to detect failure risks. When applied to
102 QA, it can potentially lead to a prioritized and targeted QA approach. Given the complex nature
103 of radiotherapy QA processes and their redundancies, we will present an unsupervised machine
104 learning tool to facilitate clustering and visualization of radiotherapy multidimensional test
105 results. We highlight a method for estimating the tolerance boundaries and performance
106 reliability of the tests by using the nontraditional Support Vector Data Description that does not
107 require explicit training as typically practiced by SVM classification, and we evaluate its
108 performance using multi-institutional data.

109

110 **II. Materials and Methods**

111

112 II.A Dataset

113 The dataset that will be used in this proposal is currently available institutionally and multi-
114 institutionally through a consortium on Automated Quality Assurance (AQA) from 8
115 participating organizations. The consortium is focused on collecting comprehensive electronic
116 portal imaging device (EPID) test results (Figure 1) from digital linear accelerators following
117 TG-142 guidelines [26,27]. A dataset takes about 15 minutes to deliver and is subsequently
118 submitted to the University of Michigan AQA database for analysis using an automated program
119 (~1 minute to run) as described by Eckhause et al. [26]. In this study, the EPID images of a
120 phantom constructed from Lucite and 2-mm diameter steel balls acting as fiducials are used to
121 determine leaf and collimator positions relative to the fixed fiducials, which are localized in the
122 image using a Canny edge detection algorithm [26]. The threshold for edge detection was
123 adjusted until all the steel balls in the phantom were detected in the image. The location of the

phantom is defined as the location of the central ball bearing. Field edges were identified by averaging the in-field and out-of-field intensities on the images and the field position was determined from the location of these edges. Leaf edges were determined according to the leaf gap size; for large gaps, the peak intensity of the gradient parallel to the leaf was used, whereas for narrow gaps (e.g., picket fence test) the positions were calculated from the local peak in the intensity profile [26]. A total of 119 independent EPID measurements of several mechanical tests of the Linac (i.e., gantry sag, field shifts, leaf positions), taken at 1-4 week intervals by 7 institutions on 8 Varian TrueBeam accelerators, were analyzed.

In order to enable visualization and analysis of the EPID QA data in higher dimensions, we will investigate the use of nonlinear kernel mapping with Support Vector with Data Description (SVDD). SVM kernel methods have been proven to produce excellent classification rates by mapping relevant input features into higher dimensional space and building optimal hyperplanes to separate low from high risk categories by maximizing the separating margin between the classes (Figure 2). Successful application of SVM to medical applications has been demonstrated in many imaging and outcome modeling studies in radiation oncology [16]. However, instead of using labeled data, which would require exhaustive annotation, we will apply a cluster labeling extension of SVM using the SVDD algorithm [28,29].

II.B Data Description (SVDD) Clustering

The basic idea of SVDD is that input data (\mathbf{x}) are mapped by a nonlinear kernel (e.g., Gaussian kernel) to the higher dimensional feature space, where one would search for the minimal enclosing hypersphere with a center a and radius R such that:

$$\min R^2 + C \sum_i \xi_i \quad (1a)$$

subject to:

$$\|\Phi(\mathbf{x}_i) - a\| \leq R^2 + \xi_i, \quad \forall i, \quad (1b)$$

where ξ_i are slack variables to allow outliers in the dataset with a regularization parameter C and $\Phi(\cdot)$ is a nonlinear mapping function (Figure 2). Using a Lagrange multiplier approach, the following conditions can be attained:

$$\|\Phi(\mathbf{x}_i) - a\| < R^2 \rightarrow \alpha_i = 0, \gamma_i = 0 \quad (2a)$$

$$\|\Phi(\mathbf{x}_i) - a\| = R^2 \rightarrow 0 < \alpha_i < C, \gamma_i = 0 \quad (2b)$$

$$\|\Phi(\mathbf{x}_i) - a\| > R^2 \rightarrow \alpha_i = C, \gamma_i > 0, \quad (2c)$$

155 where $\alpha_i \geq 0, \gamma_i \geq 0$ are Lagrange multipliers. Data points with $\alpha_i > 0$ are only needed to
 156 describe the mapping and are called support vectors (SVs), with points with $\alpha_i = C$ labelled as
 157 bounded SVs (BSVs). The solution can be obtained, as in other SVM approaches, using
 158 Quadratic Programming (QP) optimization techniques with a numerical complexity that depends
 159 on the underlying solver, which is generically between $O(n^2)$ and $O(n^3)$, where n is the number of
 160 training samples. Hence, the resulting hypersphere is given by:

$$161 \quad a = \sum_i^{N_s} \alpha_i \Phi(\mathbf{x}_i) \quad (3a)$$

$$162 \quad R^2(\mathbf{x}) = 1 - 2 \sum_i^{N_s} \alpha_i K(\mathbf{x}_i, \mathbf{x}_k) + \sum_i^{N_s} \sum_j^{N_s} \alpha_i \alpha_j K(\mathbf{x}_i, \mathbf{x}_j). \quad (3b)$$

163 For any $\mathbf{x}_k \in SV$, where N_s is the number of SVs and $K(\cdot, \cdot)$ is a kernel mapping representing the
 164 inner product: $K(\mathbf{x}_i, \mathbf{x}_j) = \Phi(\mathbf{x}_i) \cdot \Phi(\mathbf{x}_j)$. Typical kernel mapping is represented by Gaussian or
 165 radial basis functions (RBF):

$$166 \quad K(\mathbf{x}_i, \mathbf{x}_j) = \exp\left(-\frac{\|\mathbf{x}_i - \mathbf{x}_k\|}{\sigma^2}\right), \quad (4)$$

167 where σ is the width of the RBF kernel. The hypersphere, when mapped back to the input data
 168 space, can separate the data into several components, each enclosing a separate related collection
 169 of points (a cluster of QA tests) labelled following efficient graph-based [29] or dynamical
 170 system equilibrium [30,31] algorithms for preserving the topological mapping characteristics as
 171 seen in Figure 3. The labeling approach we will be using is based on decomposing the data into
 172 several disjoint groups, where each group is represented by a stable equilibrium point (SEP) to
 173 which its members are assigned the same cluster label. An SEP represents the state when the
 174 clustering system reaches equilibrium, i.e., the eigenvalues of the Jacobian corresponding to Eq.
 175 (3b) are positive yielding a stable and topologically invariant solution [30].

177 II.C SVDD Clustering Application to QA

178 There are two parameters that control the behavior of the SVDD algorithm, namely: (1) the
 179 regularization parameter (C), which defines the soft margin boundaries and controls the number
 180 of SVs and (2) the width of the RBF (σ), which controls the number of clusters in the input
 181 space. These parameters and the resulting sphere radius (R) can be used to identify the accepted
 182 confidence levels in the QA test suite, analogous to control limits in control charts but providing
 183 the important advantage of visualization in higher dimensional space. In this case, C helps
 184 identify numerical outliers (failures) and controls possible overlap between the QA testing

185 clusters while σ controls the scale at which the data points are being probed (tolerance limits).
186 Since the focus here is on visualization in higher dimensions, we fixed $C=1$ throughout the
187 experiments while σ was varied between two categories: large width in which all points fit into a
188 single cluster ($k=1$) and small width in which there are multiple clusters ($k \geq 2$). With this $C = 1$
189 setup, it also prevents BSVs (i.e., Equation 2c boundary condition). Moreover, the reported small
190 width here corresponds to the largest possible experimental σ with $k \geq 2$. For visualization in a
191 2D input space, dimensionality reduction by projection into principal component analysis (PCA)
192 is used when the dimensions are greater than 2. The software tools used are based on extensions
193 of MATLAB (Mathworks, Natick, MA, USA) for pattern recognition of data description [32]
194 and efficient SVM cluster labeling [31]. The experiments were conducted on a 64-bit Windows 7
195 machine running an Intel Xeon-E5 processor with clock speed of 3.7 GHz and 32 GB of
196 memory.

197 198 **III. Results**

199 200 III.A Gantry sag analysis by SVDD clustering

201 The gantry sags are primarily the result of gravitational torque. It is quantified as the difference
202 in the field center with respect to the phantom center (central ball bearing on the EPID image),
203 when the gantry is rotated from 0° to 180° using IEC standards [33]. Visualizing the EPID image
204 as a matrix, the differences are estimated in the in-plane and cross-plane directions of the image
205 and fed into the SVDD clustering algorithm. In Figure 4, we demonstrate the application of the
206 proposed SVDD clustering algorithm to EPID-based measurements of gantry sag. Figure 4a
207 ($\sigma=0.5$) shows a single cluster, while Figure 4b ($\sigma=0.25$) reveals two clusters, with “Cluster#2”
208 here being the outliers’ data considering the TG-142 recommended limits of gantry sag of 1 mm.
209 Using Equation 3b, the RBF mapping with large and small widths (σ) corresponds to hyperradii
210 (R) of 1.35 and 2.69, respectively. The calculations were performed in less than a second (i.e., on
211 average 0.42 ± 0.05 s for $\sigma=0.5$ and 0.43 ± 0.07 s for $\sigma=0.25$). Interestingly, the members of this
212 outlier cluster corresponded to different machines from different institutions. In this case, the
213 percentage of outliers (Cluster#2) represents 2.5% while the TG-142 isotropic box is higher at
214 8.4%. Note that the PCAs here correspond to the 0° to 180° sag measurements, respectively, and
215 demonstrate greater variation in the second principal component that corresponds to 180° .

216

217

218 III.B Radiation field shift analysis by SVDD clustering

219 The shift in the radiation field is measured in the vertical direction and is defined as the
220 difference between the radiation field positions with respect to the phantom averaged at gantry
221 angles of 90° and 270° in the in-plane and cross-plane directions of the EPID image. In Figure 5,
222 we demonstrate the application of the proposed SVDD clustering algorithm to EPID-based
223 measurements of radiation field shift with Figure 5a showing a single cluster compared to Figure
224 5b revealing four clusters. The hyperradii corresponding to large and small RBF widths were $R =$
225 1.98 and 4.85 , respectively. Three of the four clusters (Clusters #2-#4) were primarily inside the
226 TG-142 recommended limits for radiation field shift of 1 mm. The outlier cases are estimated to
227 be 2.5% while SVDD cluster analysis identified more outliers (2.5%) compared to the TG-142
228 limits (1.7%). Note that the PCAs here correspond to the 90° to 270° shift measurements,
229 respectively. Again, the calculations were performed in less than a second (i.e., on average
230 0.45 ± 0.1 s for $\sigma=0.5$ and 0.42 ± 0.06 s for $\sigma=0.25$).

231

232 III.C MLC analysis by SVDD clustering

233 The multileaf collimator data included measurements for the Varian Millennium and high
234 definition (HD) MLCs [26,27]. The Millennium MLCs consist of 120 leaves with the inner 40
235 leaves having widths of 0.5 cm and the outer leaves having widths of 1 cm. The HD MLCs
236 consist of the inner 32 leaves having widths of 0.25 cm and the outer leaves having widths of 0.5
237 cm. Measurements of Leaf offset Constancy (LoC) and transmission were available for each leaf,
238 for a total of 3486 points with the majority (83.5%) being from HD MLCs. The transmission
239 measurements were adjusted from baseline on a per leaf basis following TG-142. Previous work
240 by AQA consortium members demonstrated that the EPID-measured LoC is a comprehensive
241 and efficient way to determine if the dosimetric leaf gap (DLG) is consistent with baseline[27].
242 The procedure for the EPID measurements were adapted from the LoSasso scheme for
243 measuring DLG by using five fields: three sliding gap fields, a transmission field, and an open
244 field [27]. The 3486 LoC and transmission data points were fed into the SVDD clustering
245 algorithm. The TG-142 limit for leaf position repeatability of 1 mm was applied to the LoC and
246 evaluated, and MLC transmission was assessed against a 0.5% allowable variation from baseline.

247 Figure 6 shows the clustering results for large (Figure 6a) and small (Figure 6b) RBF widths $\sigma =$
248 2 and 0.3 with corresponding hyperradii $R = 0.35$ and 1.12 , respectively. Moreover, Figure 6b
249 identified an outlier clusters (Clusters #2) along the LoC axis (i.e., principal component #1).
250 Both the TG-142 and the SVDD estimates in this coincided with an outliers' rate of 0.34%. The
251 calculation times here increased polynomially (i.e., on average 14.4 ± 0.15 s for $\sigma=2$ and
252 174.8 ± 0.62 s for $\sigma=0.3$).

253

254

255

256 IV. Discussion

257 We have presented a machine learning approach for visualization of QA data in higher
258 dimensions and potentially for providing a mean for defining tolerance limits based on inherent
259 data characteristics and detecting outliers. The approach was based on Support Vector Data
260 Description (SVDD) with a clustering algorithm for analysis of QA data. As seen in the results,
261 this method allows for visualization of higher dimensional QA test data and interpretation of
262 non-isotropic boundary limits. The presented results were primarily qualitative, and the clusters
263 are dependent on the selection of the RBF kernel width (sphere radii). Effects of the different QA
264 tests on identifying failures could also be analyzed in this approach in a similar fashion to factor
265 loading analysis, where the effect of including/excluding a test/parameter could be visualized in
266 terms of separating annotated cases.

267

268 In this work, we have focused on applying SVDD as a visualization tool, to learn about the
269 nature of the QA data, but it can subsequently be used as an effective outlier detector as
270 presented in the results. For instance, when a deviation in gantry sag is detected, this can be
271 reported to physics/engineering for maintenance and a decision made about the needed timing of
272 maintenance and the clinical impact. [34]. In such a case the SVDD can be considered as
273 having a one-class representation of normal Linac operations and the rest would be considered as
274 outliers. In our case, we have heuristically determined the RBF width, as the largest one that
275 would result in the number of clusters ≥ 2 . We showed that a large width will result in one-
276 cluster and the that there is a width that would yield ≥ 2 , if outliers exist. To apply a more
277 autonomous approach, one would consider assembling a training data with known normal

278 operations with or without known errors (i.e., failing data) . In such a task, a grid search is
279 applied with cross-validation resampling to avoid overfitting in order to identify the hypersphere
280 radius that would minimize the classification error in a similar fashion as supervised SVM
281 training [35,36]. Moreover, the current application suggests batch processing of measurements.
282 However, a strength of SVDD is that it can be also used as an online detector by applying
283 incremental learning techniques [37,38], which would allow for efficient training and real-time
284 monitoring in a similar fashion to control charts [39].

285
286 The importance of using measurements to evaluate leaf position reproducibility, such as with an
287 EPID, rather than log files alone has previously been demonstrated by Agnew et al. [40]. A
288 number of investigators have demonstrated the importance of the accuracy of MLC leaves on
289 dosimetric accuracy of IMRT including when tolerances are considered. Others have noted that
290 pre-treatment IMRT QA methods may be inadequate at identifying different types of delivery
291 errors, especially when a gamma value is used that incorporates both distance and dose criteria
292 [41,42]. The machine learning methods applied here for an evaluation of periodic QA permit a
293 multi-dimensional evaluation of the results. The methods can also be used to identify
294 dependencies of different QA results.

295
296 The current methodology shows promise in identifying the most sensitive QA parameters and
297 quantifying the detection of outliers in a data-driven approach. In this context, SVDD can be
298 used for visualization and failure monitoring. The RBF width and/or the hypersphere radius can
299 be related to machine tolerances providing an anisotropic description of normal operations versus
300 anomalies and a mean for estimating their likelihood of occurrence and detection, which can be
301 subsequently used to rank the necessary frequency of QA tests. However, there are also
302 limitations for using RBF kernels with sphere mapping, which performed adequately for the
303 presented cases. However, other kernels/geometries or algorithms may be more appropriate in
304 other instances. Moreover, in this work we simplified the representation of TG-142 by a
305 bounding box, and the results are not intended to show preference but to provide a reference for
306 comparison only, as supervised training with annotated data may be required to evaluate and
307 establish definitive limits as discussed earlier. In addition, before applying principles such as
308 those in TG 100, further data collection and analysis is required that incorporates a longer time

309 component and includes other events such as machine breakdowns and preventive maintenance
310 on the linear accelerators. If dealing with large datasets for AQA applications becomes an issue
311 in this context, faster training algorithms of SVDD are available and can be utilized [43,44].
312 There is a richness to such datasets because the same type of detector is used for all
313 measurements. Since it is unlikely that a single institution can collect sufficient data over a few
314 years, pooling data across institutions [26] may be required to create datasets of the size required
315 to harness the power of machine learning. The application of machine learning extends beyond
316 the traditional analysis of QA results, which focuses on whether or not a test limit was met or
317 exceeded.

318 **V. Conclusions**

319 Machine learning methods based on SVDD clustering can be used as a promising tool for
320 developing automated QA methods analysis and providing insights into the effectiveness,
321 reliability, and reproducibility of such tests. Such methods offer an enhancement to the
322 information that is typically available in an individual clinic and it is an area where collaboration
323 and multi-institutional data can be valuable to establish a more efficient data-driven approach
324 rather than an opinion-driven QA program in radiotherapy.

325 **VI. Acknowledgements**

326 Part of this work was presented at the AAPM Science Council Symposium, 2017. This work was
327 supported in part by a grant from Varian Medical Systems.

328 **VII. References**

- 329 [1] BOGDANICH W. Radiation offers new cures, and ways to do harm The New York
330 Times. New York, NY: The New York Times, 2010.
- 331 [2] Kutcher GJ, Coia L, Gillin M, et al. Comprehensive qa for radiation oncology: Report of
332 aapm radiation therapy committee task group 40. Medical Physics 1994;21:581-618.
- 333 [3] Klein EE, Hanley J, Bayouth J, et al. Task group 142 report: Quality assurance of
334 medical accelerators. Med Phys 2009;36:4197-4212.
- 335 [4] Smith K, Balter P, Duhon J, et al. Aapm medical physics practice guideline 8.A.: Linear
336 accelerator performance tests. Journal of Applied Clinical Medical Physics 2017;18:23-
337 39.

- 340 [5] Followill DS, Urie M, Galvin JM, et al. Credentialing for participation in clinical trials.
341 Frontiers in Oncology 2012;2:198.
- 342 [6] Hartford AC, Galvin JM, Beyer DC, et al. American college of radiology (acr) and
343 american society for radiation oncology (astro) practice guideline for intensity-modulated
344 radiation therapy (imrt). American journal of clinical oncology 2012;35:612-617.
- 345 [7] Fitzgerald TJ, Bishop-Jodoin M, Bosch WR, et al. Future vision for the quality assurance
346 of oncology clinical trials. Front Oncol 2013;3:31.
- 347 [8] Moran JM, Molineu A, Kruse JJ, et al. Executive summary of aapm report task group
348 113: Guidance for the physics aspects of clinical trials. Journal of Applied Clinical
349 Medical Physics;0.
- 350 [9] Huq MS, Fraass BA, Dunscombe PB, et al. The report of task group 100 of the aapm:
351 Application of risk analysis methods to radiation therapy quality management. Medical
352 Physics 2016;43:4209-4262.
- 353 [10] Ford EC Evans S. Incident learning in radiation oncology: A review. Med Phys 2018.
- 354 [11] Potters L, Ford E, Evans S, et al. A systems approach using big data to improve safety
355 and quality in radiation oncology. International journal of radiation oncology, biology,
356 physics 2016;95:885-889.
- 357 [12] El Naqa I. Biomedical informatics and panomics for evidence-based radiation therapy.
358 Wiley Interdisciplinary Reviews: Data Mining and Knowledge Discovery 2014;4:327-
359 340.
- 360 [13] El Naqa I. The role of big data in radiation oncology: Challenges and potentials. In:
361 Wang B, Li R and Perrizo W, eds. Big data analytics in bioinformatics and healthcare.
362 Hershey, PA: IGI Global, 2014;pp. 163-185.
- 363 [14] Pawlicki T, Yoo S, Court LE, et al. Process control analysis of imrt qa: Implications for
364 clinical trials. Physics in medicine and biology 2008;53:5193-5205.
- 365 [15] Ford EC Evans SB. Incident learning in radiation oncology: A review. Medical Physics
366 2018;45:e100-e119.
- 367 [16] El Naqa I, Li R Murphy MJ. Machine learning in radiation oncology: Theory and
368 application. Switzerland: Springer International Publishing, 2015.

- 369 [17] Fatemeh A, David K, Jennifer GD, et al. Towards the development of an error checker
370 for radiotherapy treatment plans: A preliminary study. *Physics in Medicine & Biology*
371 2007;52:6511.
- 372 [18] Willoughby TR, Starkschall G, Janjan NA, et al. Evaluation and scoring of radiotherapy
373 treatment plans using an artificial neural network. *International Journal of Radiation*
374 *Oncology*Biology*Physics* 1996;34:923-930.
- 375 [19] Alan MK, John HG, Eric CF, et al. Bayesian network models for error detection in
376 radiotherapy plans. *Physics in Medicine & Biology* 2015;60:2735.
- 377 [20] Brown WE, Sung K, Aleman DM, et al. Guided undersampling classification for
378 automated radiation therapy quality assurance of prostate cancer treatment. *Medical*
379 *Physics*;0.
- 380 [21] El Naqa I. Detection and prediction of radiotherapy errors. In: El Naqa I, Li R and
381 Murphy MJ, eds. *Machine learning in radiation oncology: Theory and applications*, vol.
382 1. Switzerland: Springer, 2015;pp. 237-241.
- 383 [22] Valdes G, Chan MF, Lim SB, et al. Imrt qa using machine learning: A
384 multi- institutional validation. *Journal of Applied Clinical Medical Physics* 2017;18:279-
385 284.
- 386 [23] Valdes G, Scheuermann R, Hung CY, et al. A mathematical framework for virtual imrt
387 qa using machine learning. *Medical Physics* 2016;43:4323-4334.
- 388 [24] Li Q Chan MF. Predictive time- series modeling using artificial neural networks for linac
389 beam symmetry: An empirical study. *Annals of the New York Academy of Sciences*
390 2017;1387:84-94.
- 391 [25] Joel NKC, Jong Min P, So-Yeon P, et al. A machine learning approach to the accurate
392 prediction of multi-leaf collimator positional errors. *Physics in Medicine & Biology*
393 2016;61:2514.
- 394 [26] Eckhause T, Al-Hallaq H, Ritter T, et al. Automating linear accelerator quality assurance.
395 *Medical Physics* 2015;42:6074-6083.
- 396 [27] Ritter TA, Schultz B, Barnes M, et al. Automated epid-based measurement of mlc leaf
397 offset as a quality control tool. *Biomedical Physics & Engineering Express*
398 2018;4:027008.
- 399 [28] Tax DMJ Duin RPW. Support vector data description. *Machine Learning* 2004;54:45-66.

- 400 [29] Ben-Hur A, Horn D, Siegelmann HT, et al. Support vector clustering. *J. Mach. Learn.*
401 *Res.* 2002;2:125-137.
- 402 [30] Jaewook L Daewon L. An improved cluster labeling method for support vector
403 clustering. *IEEE transactions on pattern analysis and machine intelligence* 2005;27:461-
404 464.
- 405 [31] Lee J Lee D. Dynamic characterization of cluster structures for robust and inductive
406 support vector clustering. *IEEE transactions on pattern analysis and machine*
407 *intelligence* 2006;28:1869-1874.
- 408 [32] Lei B, Xu G, Feng M, et al. Classification, parameter estimation and state estimation: An
409 engineering approach using matlab. NJ, USA: John Wiley & Sons, 2017.
- 410 [33] Du W, Gao S, Wang X, et al. Quantifying the gantry sag on linear accelerators and
411 introducing an mlc-based compensation strategy. *Medical Physics* 2012;39:2156-2162.
- 412 [34] Du W, Gao S, Wang X, et al. Quantifying the gantry sag on linear accelerators and
413 introducing an mlc-based compensation strategy. *Med Phys* 2012;39:2156-2162.
- 414 [35] Theissler A Dear I. *Autonomously International Journal of Computer and Information*
415 *Engineering* 2013;7:949-957.
- 416 [36] A.G. R, Abdulla MS S. A. Lightly trained support vector data description for novelty
417 detection. *Expert Syst. Appl.* 2017;85:25-32.
- 418 [37] Oh JH, Naqa IE Yang Y. Online learning of relevance feedback from expert readers for
419 mammogram retrieval *Proceedings of the 43rd Asilomar conference on Signals, systems*
420 *and computers.* Pacific Grove, California, USA: IEEE Press, 2009; 17-21.
- 421 [38] Xie W, Uhlmann S, Kiranyaz S, et al. Incremental learning with support vector data
422 description. *2014 22nd International Conference on Pattern Recognition.* 20143904-3909.
- 423 [39] Sanghangthum T, Suriyapee S, Kim GY, et al. A method of setting limits for the purpose
424 of quality assurance. *Physics in medicine and biology* 2013;58:7025-7037.
- 425 [40] Agnew A, Agnew CE, Grattan MW, et al. Monitoring daily mlc positional errors using
426 trajectory log files and epid measurements for imrt and vmat deliveries. *Physics in*
427 *medicine and biology* 2014;59:N49-63.
- 428 [41] Kruse JJ. On the insensitivity of single field planar dosimetry to imrt inaccuracies. *Med*
429 *Phys* 2010;37:2516-2524.

- 430 [42] Steers JM Fraass BA. Imrt qa: Selecting gamma criteria based on error detection
431 sensitivity. *Medical Physics* 2016;43:1982-1994.
- 432 [43] Chaudhuri A, Kakde D, Jahja M, et al. Sampling method for fast training of support
433 vector data description. 2018 Annual Reliability and Maintainability Symposium
434 (RAMS). 2018:1-7.
- 435 [44] Cao J, Zhang L, Wang B, et al. A fast gene selection method for multi-cancer
436 classification using multiple support vector data description. *Journal of Biomedical
437 Informatics* 2015;53:381-389.

440 **FIGURE LEGENDS**

441

442 **Figure 1.** (a) The QA phantom containing small spherical fiducials. The two pieces of plastic
443 (upper left and lower right) create contrast for measuring image quality. (b) An EPID image of
444 the QA phantom. The locations of the fiducials (marked with circles) are determined with
445 automated analysis software (Reproduced from [26] with permission).

446

447 **Figure 2.** Kernel-based mapping from a lower dimensional space (X) to a higher dimensional
448 space (Z) called the feature (Hilbert) space, where non-separable classes become linearly
449 separable. In case of SVM, this mapping can be achieved using polynomials or radial basis
450 functions to create higher order features from the input data. Samples on the borders constitute
451 support vectors and they are represented by the most difficult cases to diagnose (Reproduced
452 from [16]).

453

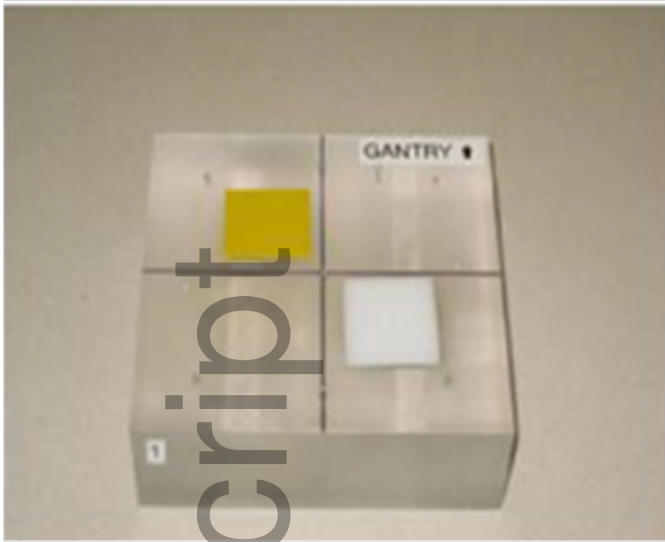
454 **Figure 3.** The main principle of the SVDD approach is that by first mapping input data from
455 potentially different characteristics (e.g., normal Linac operation versus outliers) into a higher
456 dimension and identifying the enclosing sphere (left), then re-mapping the sphere back into the
457 data space, the data points can be divided efficiently into their corresponding clusters (right)
458 [29].

459

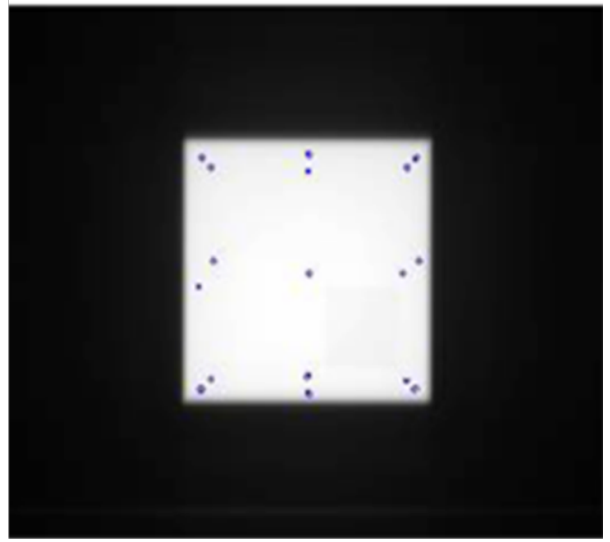
460 **Figure 4.** Gantry sag analysis using SVDD clustering. The principal components 1 and 2
461 correspond to the 0° and 180° angles, respectively. (a) Using a large Gaussian kernel width
462 ($\sigma=0.5$), it is noted that the cluster exceeds the bounds of the TG-142 recommendation (1 mm
463 box) in the input data space. (b) Using a small Gaussian kernel width ($\sigma=0.25$), it is noted the
464 presence of two clusters of measurements, with the smaller cluster representing the “true”
465 outliers per the shape of data which is anisotropic in comparison to the TG-142 recommendation.
466

467 **Figure 5.** Radiation field shift analysis using SVDD clustering with principal components 1 and
468 2 corresponding to the lateral angles (90° , 270°) angles, respectively. (a) Using a large Gaussian
469 kernel width ($\sigma=0.5$), the cluster encloses all measurements with the red circles showing the
470 support vectors (boundary points). (b) Using a small Gaussian kernel width ($\sigma=0.25$), the
471 presence of two distinct classes of measurements is noted primarily related to variations in the
472 second principal component (270° measurements).
473

474 **Figure 6.** MLC shift analysis using SVDD clustering, the principal components 1 and 2
475 correspond to LoC and transmission respectively with the dashed rectangle representing TG-142
476 limits. (a) Using a large Gaussian kernel width ($\sigma=2$), it is noted that the cluster encloses all
477 measurements, with the red circles showing the support vectors (boundary points). (b) Using a
478 small Gaussian kernel width ($\sigma=0.3$), it is noted the presence of 2 regions (clusters) in the data in
479 the LoC direction.

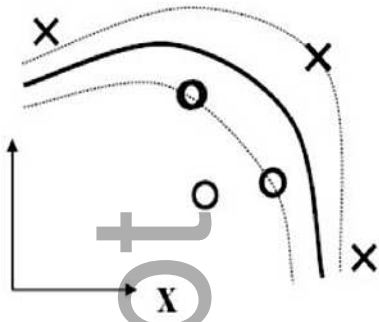


(a)



(b)

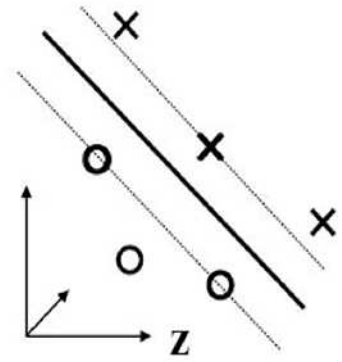
mp_13433_f1.tiff



$$\Phi(\cdot)$$

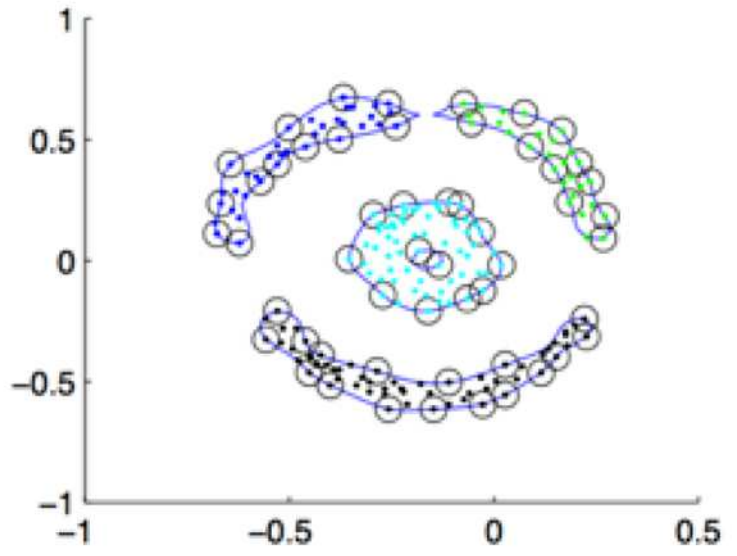
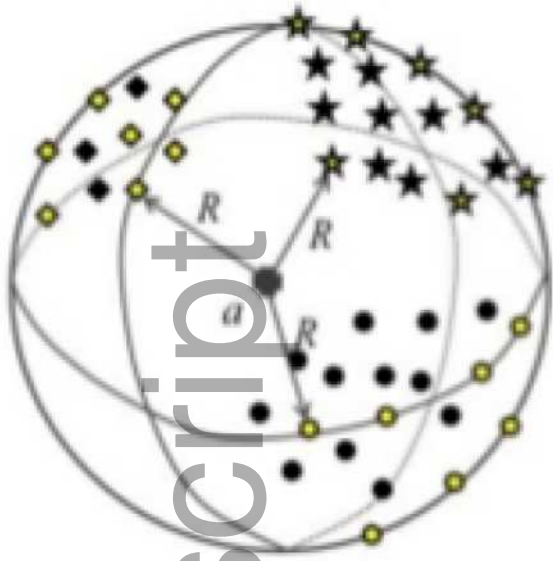
\longrightarrow

$$z = \Phi(x)$$

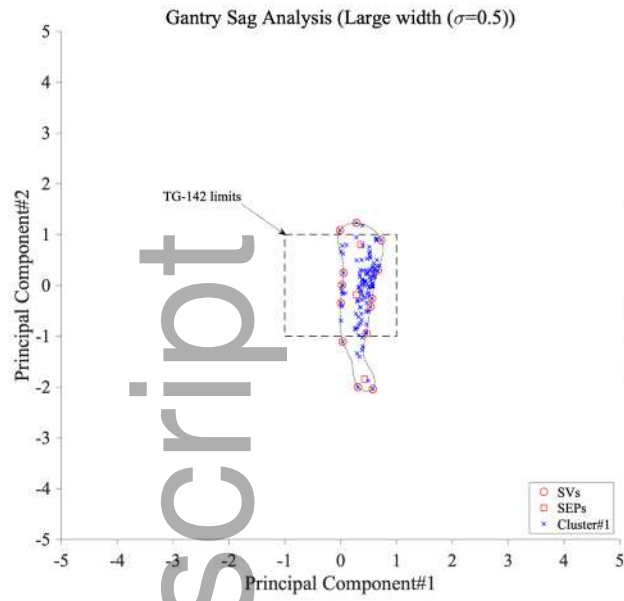


mp_13433_f2.tiff

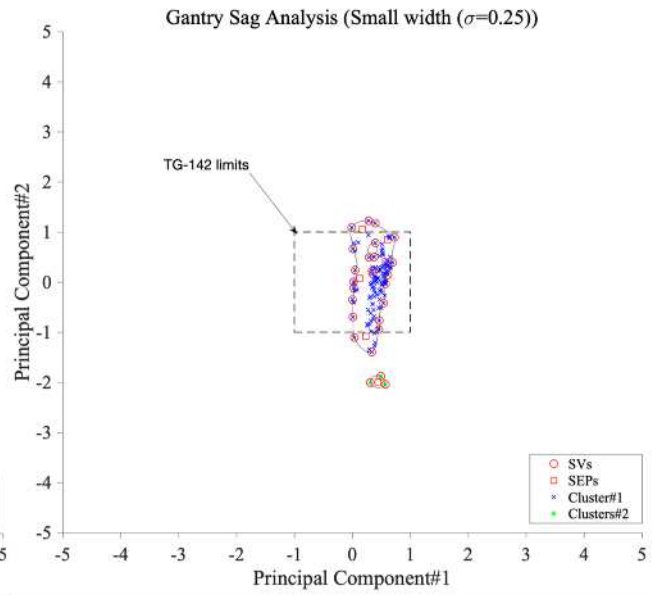
Author Manuscript



mp_13433_f3.tiff

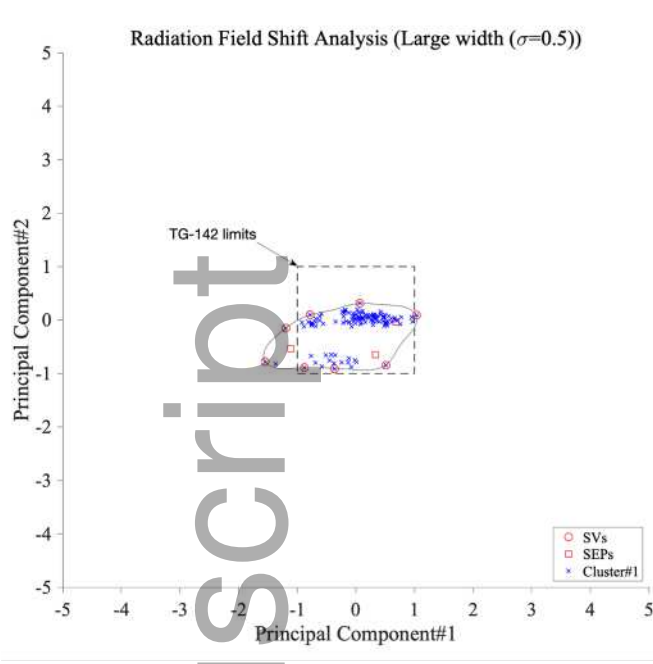


(a)

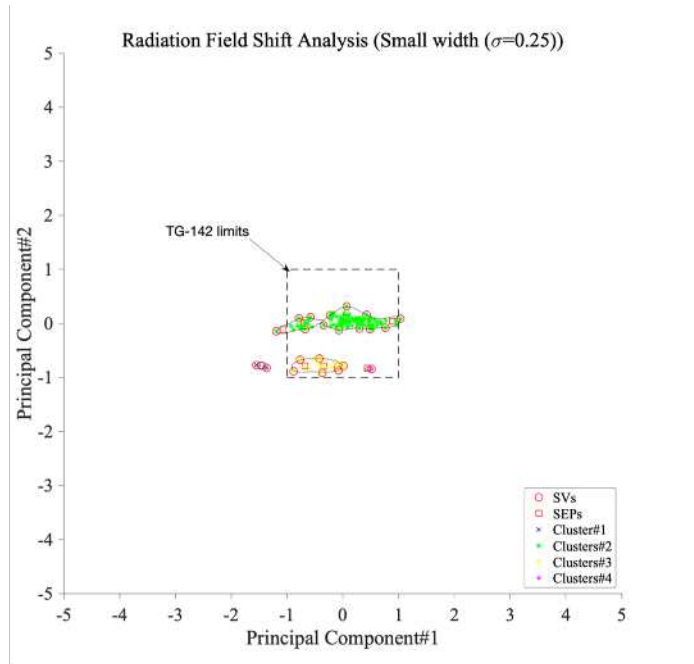


(b)

mp_13433_f4.tiff

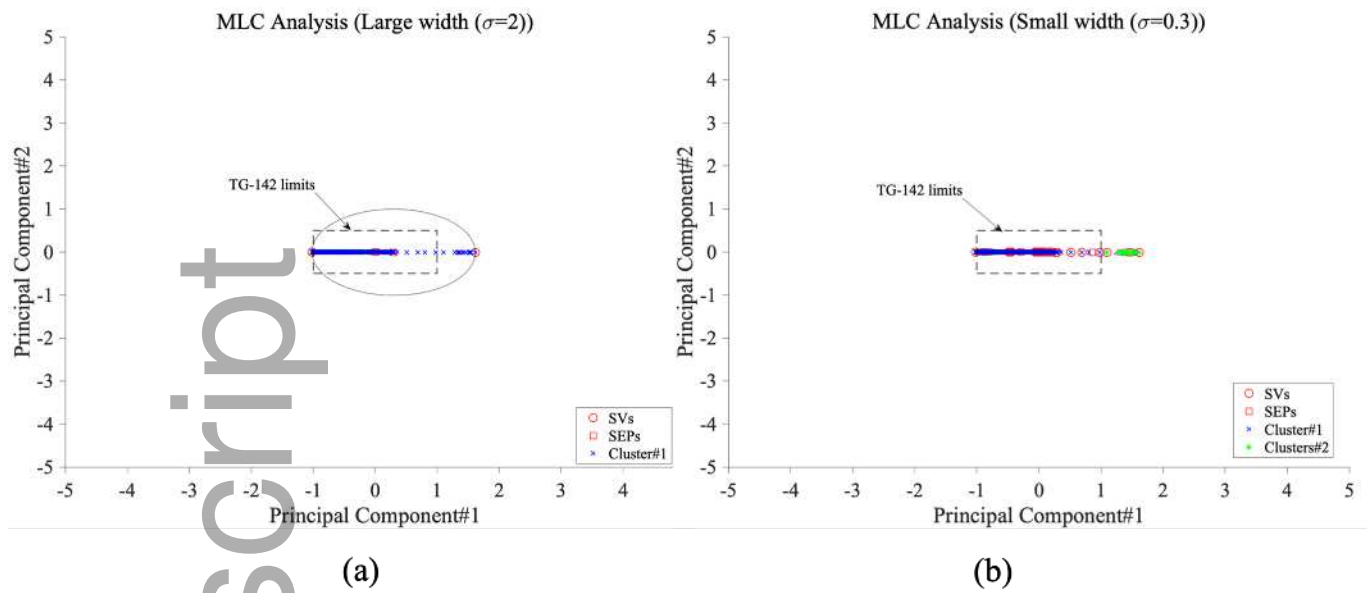


(a)



(b)

mp_13433_f5.tiff



mp_13433_f6.tiff